International Journal of Heat and Mass Transfer 64 (2013) 773–782

Contents lists available at SciVerse ScienceDirect

International Journal of Heat and Mass Transfer

journal homepage: www.elsevier.com/locate/ijhmt

Unexpected natural convection heat transfer for small Rayleigh numbers in external geometry

Margaritis Kostoglou [1], Sotiris P. Evgenidis [2], Thodoris D. Karapantsios *

Division of Chemical Technology, School of Chemistry, Aristotle University, University Box 116, 541 24 Thessaloniki, Greece

ARTICLE INFO

Article history:
Received 6 July 2012
Received in revised form 25 January 2013
Accepted 7 May 2013
Available online 3 June 2013

Keywords:
Natural convection
Gravitational acceleration
Conduction
Rayleigh number
Spheroidal heater
Miniature heater

ABSTRACT

Recently, analysis of experimental data of heat transfer from submillimeter heaters at different levels of gravitational acceleration revealed a peculiar behavior of the natural convection Nusselt number (Kostoglou et al. (2011) [4]). In particular, it was found that no natural convection heat transfer appears for Rayleigh numbers smaller than a threshold value in external geometry which contradicts the common belief that this is possible only in internal (confined) geometry. This issue is studied further herein. Additional experiments are performed with higher resolution in the parameters' range and also with other liquids of varying thermophysical properties to clarify the situation. The analysis of the present data confirms the findings of the previous work and leads to a more detailed picture for the relation between Nusselt number and Rayleigh number. The relation found is against existing correlations and existing experimental evidence in literature (acquired at terrestrial conditions). Numerical simulations of natural convection in the employed external geometry are performed in order to explain the discrepancy between the behavior of the present measurements and existing correlations. It seems that the effect of varying gravitational acceleration is rather complex and cannot be accounted simply by a change in the Rayleigh number.

1. Introduction

Natural convection is a very important mechanism for heat transfer from geological scale to micron size systems used in engineering. A large part of the huge literature on the subject refers to large Rayleigh (*Ra*) number applications typical for the size scale of mechanical engineering machinery. Much of the above work is on special techniques for the treatment of the corresponding mathematical problem amenable to approximate solutions even before the explosion of the computer power in last decades [1]. The remaining part of literature refers mainly to chemical engineering equipment (packed beds) and electronic engineering equipment (cooling of electronic components) and is also very extensive on both experimental and theoretical efforts [2,3].

Small *Ra* numbers are met in systems having small characteristic sizes or/and small temperature differences. Another domain where small *Ra* numbers are met is microgravity (space) research since *Ra* scales linearly with the value of gravitational acceleration. For internal (confined or closed domain) geometries it is well known that a critical *Ra* number (below which no natural convection is observed) may exist depending on the specific geometry. However, serious deviations have been reported even for such geometries. For instance, the present authors working with water and glycerine suggested the existence of a critical Rayleigh number which is not compatible with the theory for the employed external (unconfined or open domain) geometry [4].

Over the last years, we have been investigating thermal degassing of liquids [5–8] using miniature (submillimeter) heaters. In an effort to decouple bubble growth from buoyancy effects we did several experiments in the low gravity environment of parabolic flights during the 25th, 26th, 35th and 38th European Space Agency (ESA) Parabolic Flight Campaigns (PFC). However, results from those experiments displayed a significant deviation from theoretical predictions indicating a possible contribution from residual natural convection probably due to the poor low-g conditions in parabolic flights [9,10].

In an attempt [4] to test this hypothesis, heat transfer experiments were conducted during the 49th ESA PFC in degassed water and glycerol aiming to investigate the effect of the different gravity levels (~0, 1, ~1.6 g) attained during parabolas on the development of a thermal boundary layer around miniature spheroidal heaters in a quasi-infinite (open domain) geometry. An interesting result was obtained: a *threshold Rayleigh* number for natural convection was found below which no contribution to heat transfer

* Corresponding author. Tel./fax: +30 2310997772.
E-mail addresses: kostoglu@chem.auth.gr (M. Kostoglou), sevgenid@chem.auth.gr (S.P. Evgenidis), karapant@chem.auth.gr (T.D. Karapantsios).
[1] Tel.: +30 2310997767; fax: +30 2310997759.
[2] Tel.: +30 2310997798; fax: +30 2310997759.

0017-9310/$ - see front matter © 2013 Elsevier Ltd. All rights reserved.
http://dx.doi.org/10.1016/j.ijheatmasstransfer.2013.05.019

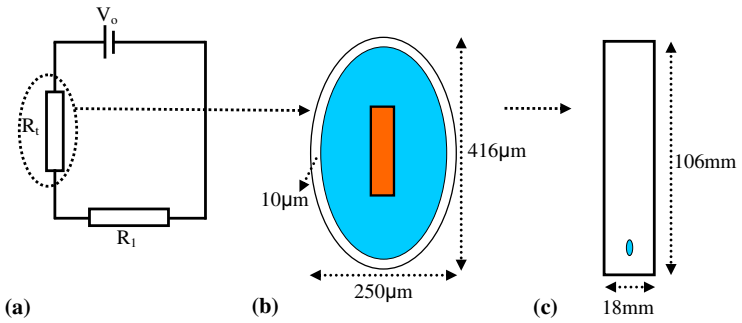

Fig. 1. Schematic representation of the experimental system: (a) Electrical circuit, (b) Heater geometry and (c) Sample cell geometry.

could be measured. At first glance, this is contrary to predictions of existing heat transfer theories and correlations for external (open domain) geometries which predict a continuous, progressively increasing, contribution of natural convection to heat transfer with respect to gravity (starting from zero gravity). However, it must be stressed that from a fluid mechanics point of view it was not possible to say if there was natural convection (motion of fluid) around the heaters. What it was argued is that below a threshold *Ra* there was no measurable effect on heat transfer. Yet, to avoid confusion with the conventional knowledge for closed domains we adopted the term *threshold Ra* instead of *critical Ra*. Interestingly, we were unable to find in literature experimental evidence for very small *Ra* in external geometries where gravity conditions were adjustable.

In a further effort to discriminate between the effects of gravity level and liquid properties on the existence of a threshold *Ra*, a new series of experiments was conducted in the 50th ESA PFC [11]. First, a dense matrix of tests with water at different heating powers was performed as a reference and also as a reproducibility check with prior PFCs tests. Then, tests were performed with FC-72 (a liquid refrigerant) because of its much lower kinematic viscosity than water which allows more profound appearance of natural convection during different g-levels. Finally, tests were also conducted with packed beds and dense suspensions of two size classes of polystyrene particles in water in order to introduce different degrees of heterogeneity in the liquid phase and therefore examine in another way the effect of liquid properties. These experiments confirmed that there is a threshold before natural convection appears, with natural convection being more profound in FC-72 than water. In addition, closely packed particles suppressed entirely natural convection but in dense particle suspensions transient convection currents prevailed.

This work elaborates on the analysis of the raw experimental data of [11] in order to pursue further insight on the subject. The present analysis is strictly limited to water and FC-72 data since the situation is far more complex with packed beds and particle suspensions which are left to examine at a next stage. The structure of the present work is the following: First, experimental data are presented. Then an analysis of the experimental data is performed. In doing this the focus is on the steady state temperature of the miniature heater in the microgravity and hypergravity periods attained during parabolas. From these temperatures an estimation of the natural convection contribution on heat transfer is made. Finally, several numerical simulations of the heat transfer problem for a step change in the heater's temperature are presented in an attempt to interpret the experimental results (transient and steady state).

2. Experimental results

The raw data of [11] for water and FC-72 are employed for the present analysis. Fig. 1 displays the schematic representation of the employed miniature spheroidal heater as well as the employed electrical circuit for heating and the heaters position at the lower end of the cylindrical sample cell containing the working fluid. The heater consists of a heat source (orange[3] in Fig. 1b) embedded in a metallic body (blue in Fig. 1b) which is surrounded by a thin (~10 μm) quartz layer.

The temperature and power of the heater can be calculated as follows. If voltage drop is measured across a reference constant resistance R_1 and R_t is the internal ohmic resistance of heater, then the current in the circuit is $I = V_o/(R_t + R_1)$ and V_R at the edges of R_t is:

$$V_R = V_o - IR_1 = V_o\left(1 - \frac{R_1}{R_1 + R_t}\right) \tag{1}$$

Solution of the above equation for R_t provides the resistance value of the heater. The heater temperature value, T_t, is computed by inversion of the function $R_t(T_t)$ which is taken from the calibration of the heater's resistance against known temperatures. In addition, the delivered power of the heater, P, is a function of $R_t(T_t)$:

$$\begin{aligned} P = V_R I &= V_o^2\left(1 - \frac{R_1}{R_1 + R_t}\right)\left(\frac{1}{R_1 + R_t}\right) \\ &= \frac{V_o^2}{R_1}\left(1 - \frac{1}{1 + R_t(T_t)/R_1}\right)\left(\frac{1}{1 + R_t(T_t)/R_1}\right) \end{aligned} \tag{2}$$

The power of the heater as a function of the heater temperature is shown in Fig. 2 for several values of V_o employed in the experiments. Data of the heater temperature, T_t, vs. heating time are displayed for water (Fig. 3a) and FC-72 (Fig. 3b) at different applied voltages. Measurements start (0 s) during the low gravity phase and extend in the succeeding hypergravity phase. A typical curve of the onboard gravitation acceleration (courtesy of ESA) is also displayed in the figures. The experimental conditions for each experiment are shown in Table 1. Two steady state temperatures are given in the Table for each experiment. The 1st steady state temperature corresponds to the value attained at the end of the microgravity period whereas the 2nd steady state temperature corresponds to the value attained at the end of the hypergravity period. These temperatures are computed by averaging over a period of 2–5 s to remove the measurement noise. The missing values of the hypergravity (2nd) steady state temperature in the Table are because in these experiments there was no observable temperature variation (given the experimental noise) when going from microgravity to hypergravity.

3. Discussion and interpretation of experimental results

Experimental results are analyzed qualitatively first and then quantitatively. For both liquids the temperature of the heater

[3] For interpretation of color in Fig. 1, the reader is referred to the web version of this article.

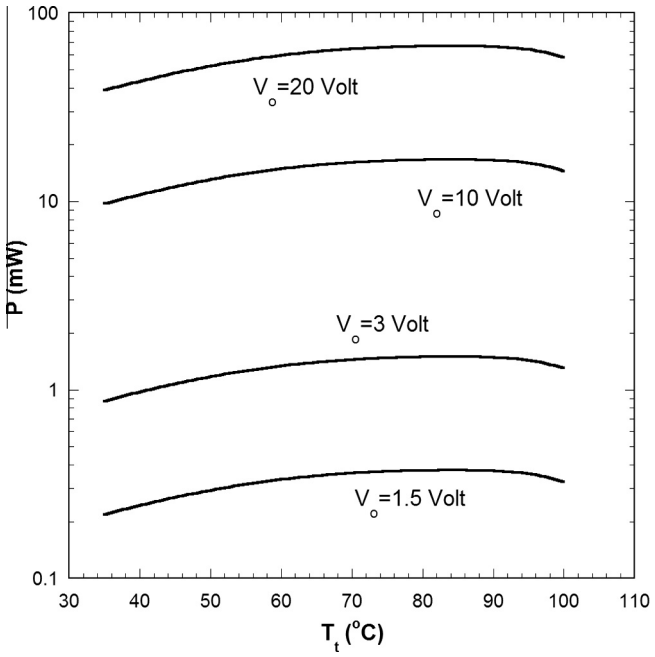

Fig. 2. Heater energy source strength P vs. heater temperature T_t.

increases fast at the beginning of the heat pulse and slower later towards an asymptotic steady state value. When the temperature almost reaches a 1st steady state, the gravitational acceleration climbs rapidly to a hypergravity value and as a result the temperature drops fast towards a 2nd steady state. At first glance, the 1st steady state value corresponds to heat transfer from the heater to the liquid by conduction and the 2nd steady state value to heat transfer by natural convection. The difference between the two steady state temperatures is clearly due to the onset of natural convection. For water and low power heat pulses this difference is essentially zero and increases disproportionally to the difference between the initial temperature of the liquid, T_o, and the 1st steady state temperature, T_{1ss}, (Table 1). On the contrary, for FC-72 the difference between the two steady state temperatures ($T_{1ss} - T_{2ss}$) is proportional to the difference ($T_{1ss} - T_o$). Since these experimental findings do no obey usual correlations for natural convection we will not directly compare existing theories with experiments but we will extract first from the experiments as much information as possible.

At steady state the temperature of the heater fulfills the condition

$$P(T_t) = Q(T_t) \tag{3}$$

where P is the power generated at the heater and Q the heat dissipated from the heater to the liquid. It is noted that the above condition corresponds to a pseudo-steady state since the liquid temperature increases during heating. An integral heat balance taking into account the heat pulse strength, the duration of the experiment and the volume of the liquid in the cell, reveals that the average temperature increase in the cell is very low (much less than 0.1 °C) so the pseudo-steady state assumption is valid. The next step is to estimate the heat dissipated from the heater. At first stage only conduction is considered. The thermal conductivity k_m of the metallic part of the heater is excessively higher than the thermal conductivity k_q of the quartz and of the liquid so the temperature can be assumed uniform in the inner body of the heater (T_t). The protective quartz layer of thickness δ is thin with respect to the curvature radius of the heater so it can be assumed planar. The heat flux through

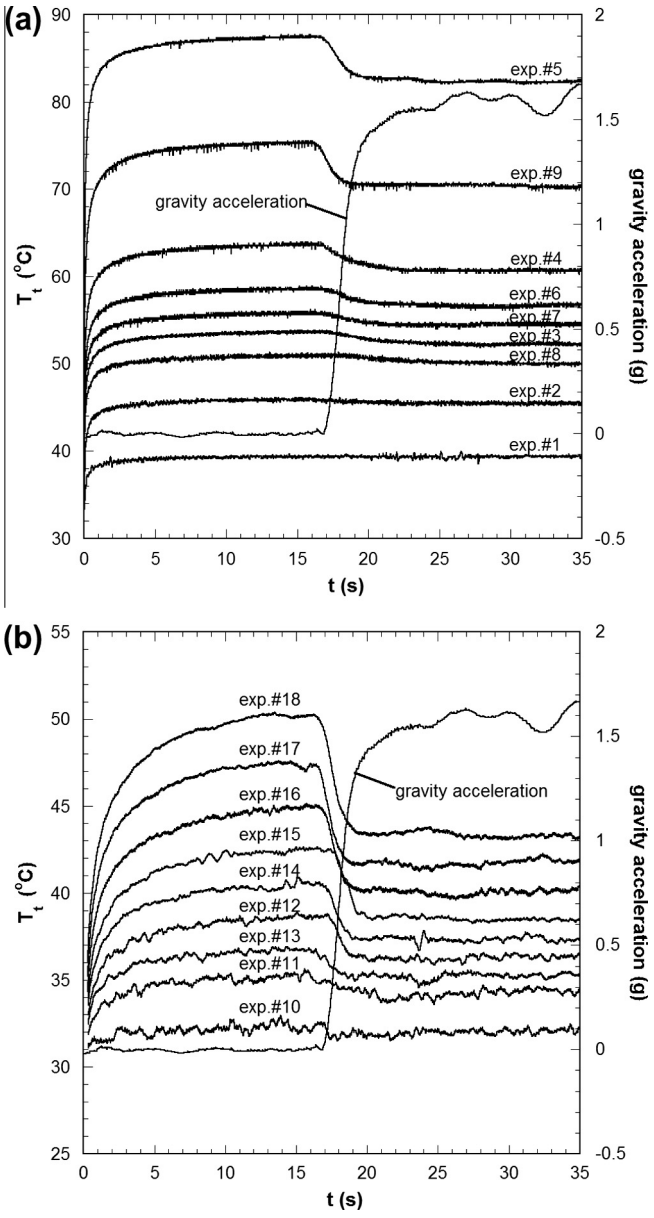

Fig. 3. Heater temperature, T_t, evolution for several V_o values (a) water (b).

this film is given as (A is the surface area of the heater and T_i its outer surface temperature).

$$\frac{Q_1}{A} = \frac{k_q}{\delta}(T_t - T_i) \tag{4}$$

The dissipated heat from the outer surface of the heater can be found by solving the steady state heat conduction equation. This is an elliptic partial differential equation of Laplace type that can be solved analytically in prolate spheroidal coordinates. The analytical solution leads to the following rate of heat transferred from the heater to the liquid [12]

$$Q_2 = \frac{4\pi\sqrt{\alpha^2 - b^2}k(T_i - T_o)}{\ln\left(\coth\left(\frac{1}{4}\ln\left(\frac{\alpha+b}{\alpha-b}\right)\right)\right)} \tag{5}$$

where α, b are the large and the small semi-axes of the heater and k is the liquid conductivity.

Under steady state conditions it should be $Q_1 = Q_2$. This equation can be solved for T_i which is replaced in Eq. (5) to give the final expression for the conduction heat losses of the heater:

Table 1
Experimental conditions and measured steady state temperatures. T_o is the initial temperature of the liquid before heating.

Exp. #	V_o (V)	T_o (°C)	Liquid	Microgravity 1st steady state T_{1ss} (°C)	Hypergravity 2nd steady state T_{2ss} (°C)
1	9.3	30.8	Water	39.5	–
2	11.3	31.2	Water	45.6	–
3	13	31.5	Water	53.5	52.1
4	15	31.6	Water	63.8	60.8
5	19.2	31.7	Water	87.4	82.3
6	14	31.7	Water	58.4	56.5
7	13.5	31.8	Water	55.6	54.1
8	12.5	31.8	Water	50.9	50.1
9	17	31.8	Water	75.5	70.7
10	1.4	30.5	FC-72	32.3	–
11	2.1	31.2	FC-72	35.5	34.3
12	2.6	31.4	FC-72	38.5	36.1
13	2.3	31.4	FC-72	36.6	35.1
14	2.9	31.4	FC-72	40.5	37.5
15	3.1	31.4	FC-72	42.4	38.6
16	3.3	31.4	FC-72	45	40.2
17	3.5	31.4	FC-72	47.3	41.4
18	3.7	31.5	FC-72	50.2	43.4

$$Q = \left(\frac{\ln\left(\coth\left(\frac{1}{4}\ln\left(\frac{\alpha+b}{\alpha-b}\right)\right)\right)}{4\pi\sqrt{\alpha^2-b^2}k} + \frac{\delta}{Ak_q} \right)^{-1} (T_t - T_o) \tag{6}$$

where the surface area of the prolate spheroid is computed as:

$$A = 2\pi\left(b^2 + \frac{\alpha b \arccos(b/\alpha)}{\sin(\arccos(b/\alpha))} \right) \tag{7}$$

The next step is to include natural convection in the above analysis. According to literature, the total Nusselt number for heat transfer from an object to the surrounding liquid in an external geometry (open domain) is given as a linear combination of the conduction and natural convection contribution [13]. In fact, in some cases a generalized non-linear addition is proposed but the suggested exponents are pretty close to unity leading to a practically linear approach [14,15]. So, $Nu = Nu_{cond} + Nu_{natconv}$. A simple modification leads to $Nu/Nu_{cond} = 1 + H$ where H is the ratio of natural convection to conduction contribution. Employing the above definition of H and using equations (2), (3), and (6) the following non-linear algebraic equation arises which must be solved for an equilibrium value of T_t if H is known or alternatively for H if an equilibrium T_t is known.

$$\frac{V_o^2}{R_1}\left(1 - \frac{1}{1+R_t(T_t)/R_1}\right)\left(\frac{1}{1+R_t(T_t)/R_1}\right) = Q$$
$$= \left(\frac{\ln\left(\coth\left(\frac{1}{4}\ln\left(\frac{\alpha+b}{\alpha-b}\right)\right)\right)}{4\pi\sqrt{\alpha^2-b^2}k(1+H)} + \frac{\delta}{Ak_q} \right)^{-1} (T_t - T_o) \tag{8}$$

The crucial dimensionless number accounting for the extent of natural convection in a heat transfer problem is the Rayleigh number Ra defined as

$$Ra = \frac{\rho^2 c_p \gamma \beta (T_t - T_o) L^3}{k\mu} \tag{9}$$

where ρ is the density of the liquid, c_p its specific heat capacity, k its thermal conductivity, μ its dynamic viscosity, β its coefficient of thermal expansion, γ the generalized gravitational acceleration and L a characteristic size of the heater. For the particular case treated here as characteristic size is taken the arithmetic mean of the two spheroid diameters ($L = \alpha + b$). It is considered to be a more appropriate choice than the large diameter considered as L in our previous work [4]. According to equation (9) Ra increases linearly with the difference between heater temperature, T_t, and initial liquid temperature, T_o. The situation, however, is more complex due to the temperature dependence of the physical properties appearing in Eq. (9). The question is at which temperature these physical properties should be computed in Eq. (9) given that the temperature around the heater varies from T_t to T_o? Typical correlations in literature employ weighted averages of T_t and T_o.

In order to display better the whole possible range of Ra values as a function of the heater temperature, the parameters are computed at three temperatures (let us call T_c the parameter computation temperature) $T_c = T_o$, $T_c = T_t$ and $T_c = T_f = (T_t + T_o)/2$. The curves Ra vs. T_t for the three choices of T_c are shown in Fig. 4 for water and in Fig. 5 for FC-72 (T_o is chosen as 31.5 °C to be close to the present experimental conditions). It is noted that in our previous work [4] for glycerol as test fluid the Ra numbers were much smaller than those of water. The FC-72 used here has Ra numbers an order of magnitude larger than those of water. Most of the physical parameters of water and FC-72 are comparable. The difference to

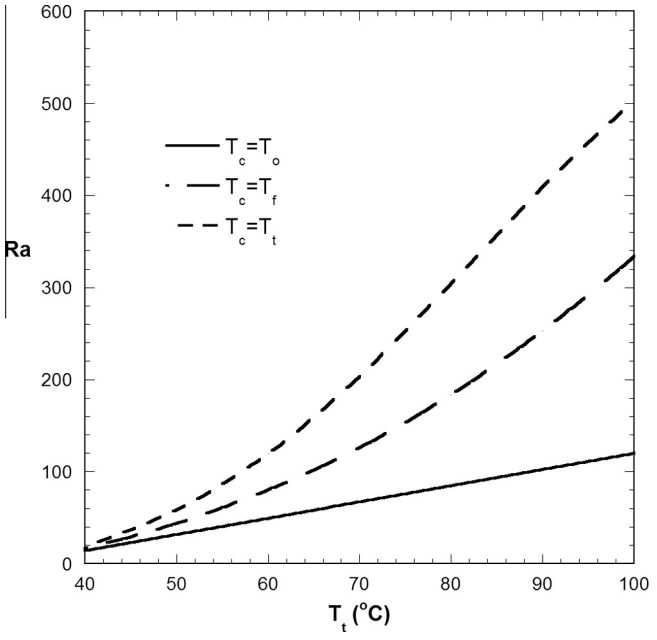

Fig. 4. Computed Ra number vs. temperature of heater for water using three values of the characteristic temperature T_c for physical property computation i.e., T_o, T_f and T_t.

the corresponding *Ra* numbers is due to the thermal conductivity (lower for FC-72) and thermal expansion coefficient (higher for FC-72). There is a considerable variation of *Ra* with T_c for the case of water (Fig. 4). Yet, taking $T_c = T_f$ in (9) can still lead to quantitative but not qualitative deviations from the theoretically optimal *Ra* number arising when taking into account the exact temperature field. On the other hand, the variation of *Ra* with T_c for FC-72 is small and the assumption of parameters without temperature dependence is an acceptable approximation.

In order to proceed to the analysis of experimental data, it is first assumed that during the low gravity period of parabolas the effect of natural convection (due to g-jitters) is negligible. This assumption will be tested later in the analysis. According to the above assumption the 1st steady state temperature, T_{1ss}, is dictated by conduction and can be found by setting $H = 0$ in Eq. (8), solving for T_t and comparing the theoretical and experimental T_t at long times. A different way is followed here since the focus is on the study of natural convection. To appraise experimental errors in the calculation procedure, T_t in equation (8) is assumed as the experimental one and the equation is solved for the value of conductivity *k*. The literature value of the conductivity of fluids (computed at T_f) with respect to the temperature T_t and the corresponding values taken by the above procedure are shown in Fig. 6. It is noted that the FC-72 conductivity values are shown multiplied by five for clarity of presentation. The differences between literature and experimental values are due to experimental errors (max error less than 1.5%) and they are acceptable for the purposes of the present work.

The experimental value of conductivity and the 2nd steady state temperature T_{2ss}, (corresponding to the hypergravity period) are employed in equation (8) to estimate the parameter *H*. The values of *H* derived in this way are presented vs. the *Ra* number of the particular experiment (computed at $T_c = T_f$) in Fig. 7. For water, the findings of our previous work [4] are fully supported by the new data comprising a denser grid of experimental points. It seems that the factor *H* is negligibly small up to a threshold value of Rayleigh number (let us call it Ra_{th}) after which it starts increasing abruptly. It is not sure that the value of *H* is absolutely zero (no natural convection at all) for $Ra < Ra_{th}$. There is a probability that for such a small *Ra* value the created temperature difference is of the order of the temperature measurement noise. More important is the overall shape of the *H* vs. *Ra* curve than the local arithmetic details. The functional form used in the previous work [4] $H \approx 0$ for $Ra < Ra_{th}$ and $H = p_1(Ra - Ra_{th})^{p_2}$ is confirmed by the present data. The best fit for the water data leads to $Ra_{th} = 40$, $p_1 = 0.01749$, $p_2 = 0.377$ (fit1 in Fig. 7). The presently estimated Ra_{th} is different than in the previous work ($Ra_{th} = 70$) but the difference is superficial and it is due to the different characteristic length used in the *Ra*

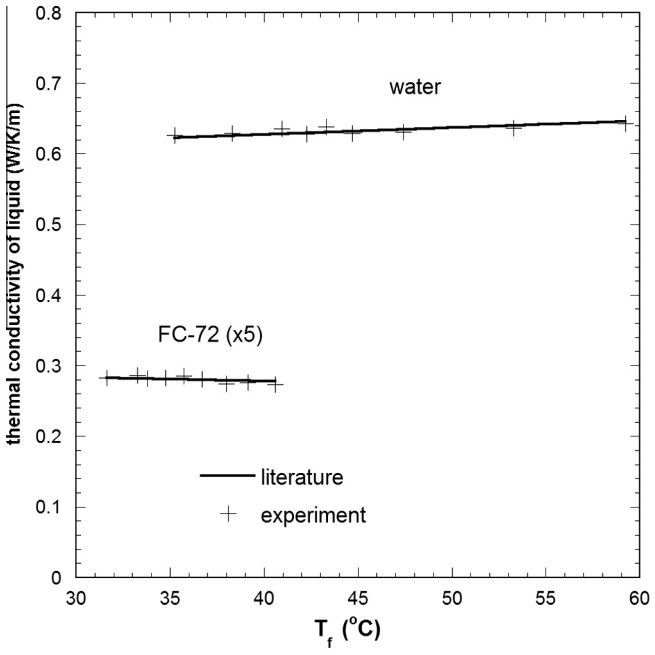

Fig. 6. Thermal conductivities of water and FC-72, estimated from the steady state temperatures of the heater, compared to literature values (computations at T_f).

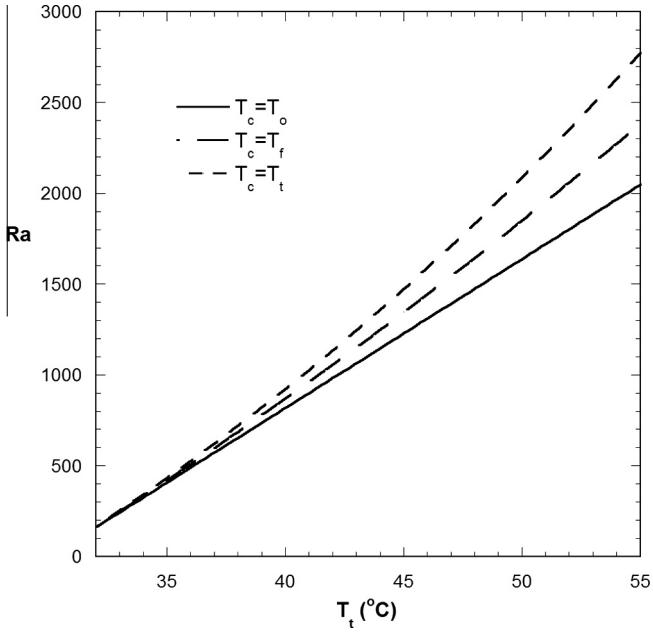

Fig. 5. Computed *Ra* number vs. temperature of heater for FC-72, using three values of the characteristic temperature T_c for physical properties computation i.e., T_o, T_f and T_t.

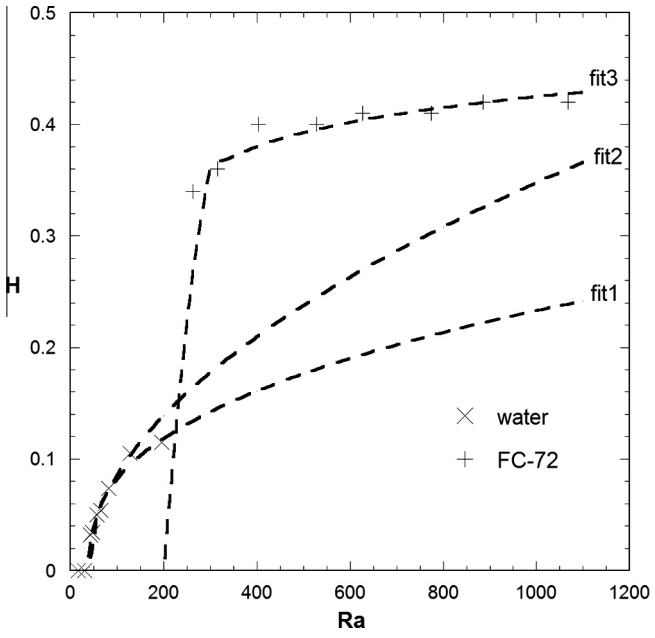

Fig. 7. Ratio of natural convection to conduction contribution heat transfer H vs. Rayleigh number for water and FC-72. Several fitting curves explained in the text are shown.

number definition. To urge a discussion below, an alternative best fit is shown in Fig. 7 obtained by excluding the last (higher *Ra*) experimental water point (fit2, $Ra_{th} = 35$, $p_1 = 0.00975$, $p_2 = 0.52$).

While it was expected that the data for FC-72 would be complementary to those of water, their analysis led to surprising results. The factor *H* increases very slowly with *Ra* number. An attempt was made in Fig. 7 to determine a best fit curve similar to that used for water (fit3, $Ra_{th} = 200$, $p_1 = 0.2488$, $p_2 = 0.08$). The curve is completely incompatible with the one computed for water (larger Ra_{th} and smaller exponent p_2). The best fit curve for FC-72 (fit3) has no real physical meaning (it is drawn just to check compatibility) since the fluctuations in the temperature measurements for the lowest $V_o = 1.4$ V in Fig. 3b are comparable to the temperature drop when going from microgravity to hypergravity and so do not permit a safe indication of Ra_{th}. The curve fit2 for water approaches the FC-72 data but its *Ra* dependence is much higher than FC-72 and fit1, so it does not seem to be a feasible alternative. The different behavior observed for water and FC-72 does not constitute an inconsistency regarding the existence of Ra_{th} since all the data for FC-72 refers to *Ra* numbers larger that the Ra_{th} computed from water experiments. In the same way, the glycerol data in [4] refer to *Ra* numbers smaller than Ra_{th} for water, as would be expected for $H = 0$ found for glycerol. So, the experiments for the three test fluids are consistent regarding the existence of Ra_{th}. It must be emphasized, though, that the curve shown in Fig. 7 to fit the FC-72 data is presented only for completeness and by no means suggests that $Ra_{th} = 200$ since experimental noise is substantial for FC-72 at low heat powers. In fact, the FC-72 data do not suggest any specific value for Ra_{th} but still they imply the existence of Ra_{th}.

The above direct experimental findings for the factor *H* will be discussed now in view of the existing correlations and experimental results on the subject. The general correlation for *H* in literature (derived from the actual correlation between Nusselt number and *Ra*, *Pr*) is

$$H = C(Pr)Ra^m \tag{10}$$

where *Pr* is the Prandtl number. It is noted that the above correlation refers to an external (open domain) geometry for which even a negligibly small density difference can create fluid motion, i.e., a threshold or critical *Ra* does not exist. The situation is different in internal (closed domain) geometries where the viscous forces created by fluid recirculation must overcome a lower limit in the density reference for the onset of fluid motion. The discussion here is restricted to the case of laminar flow (based on the fact that the maximum experimental value of *Ra* is around 1000, far beyond the transition to turbulence limit). The exponent *m* is usually constant but in some cases a weak dependence on *Ra* has been proposed [16]. The generally accepted value for *m* for the region of *Ra* treated here is $m = 0.25$. Several suggested forms can be found in literature for the function *C*. A typical one is given in [17]:

$$C = 0.28\left(\frac{Pr}{0.846 + \mathrm{Pr}}\right)^{1/4} \tag{11}$$

The exact form of $C(Pr)$ is not really important due to the limited variation of the function with respect to its argument. All suggested relations like (11) predict that *C* does not differ more than 10% among all liquids (excluding liquid metals).

In general, *Pr* is a function of temperature. This means that *Pr* differs from experiment to experiment in Fig. 7 and the different than 0.25 exponents found in the best fit curves accommodate the effect of *Pr* number. A possible explanation of the gap between *H* values of water and FC-72 shown in Fig. 7 could be the difference in the *Pr* number of the two liquids. In order to better illustrate this difference, the *Pr* number for water and FC-72 vs. temperature T_t is displayed in Fig. 8 ($T_o = 31.5$ °C). In any case, the variation of the

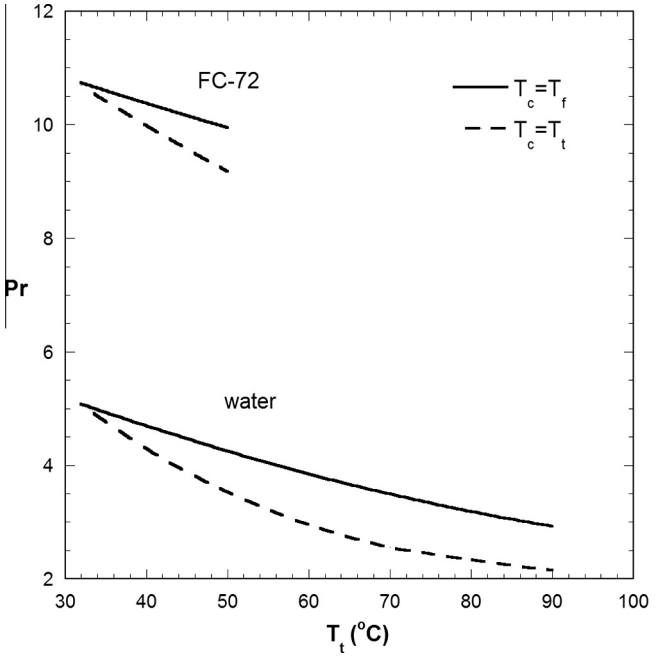

Fig. 8. Variation of Prandtl number with heater temperature T_t (properties taken at T_f).

function *C* among the FC-72 experiments is less than 1% and among water experiments less than 4%. Also the difference of parameter *C* between the two fluids does not exceed 6%. The above shows that *Pr* variation (based on existing theories) cannot explain the non-typical behavior shown by the present experimental data. Another important aspect of the present experimental evidence is the existence of a threshold Rayleigh number which is not compatible to equation (10) that predicts a finite contribution of natural convection for any value of *Ra*.

A discussion on the validity of literature Eqs. (10) and (11) is imperative here in order to assess the source of discrepancies. Eq. (10) has been verified extensively against numerical simulations and against experimental data [16]. A literature survey reveals that most of the experiments for external natural convection were performed in air (e.g. [18]). The experiments in water were typically performed in a *Ra* range with larger values than those examined here (e.g. [19,20]). The experiments in liquids in the range of physical parameters examined here seem to be limited [16]. Nevertheless, we are not aware of any literature report claiming that something much different than equation (10) holds for different physical parameters than those experimentally tested. On the other hand, the experimental data taken here are very consistent. The experiments are reproducible, the whole set-up is simple in conception and its components have been tested carefully. The good prediction of the thermal conductivity of liquids in Fig. 6 at low gravity conditions (only conduction present) is a stringent test for the correctness of the measuring approach. The main aspects of the experimental findings (e.g. existence of Ra_{th} and difference between water and FC-72) can be observed directly at the recorded temperatures without any further quantitative analysis.

We stress here that to our knowledge this is the only experimental study of this type (studying heat transfer around miniature heaters with varying gravitational acceleration) and this allows independent estimation of the conduction and natural convection contributions. In terrestrial conditions, heat transfer begins with a heat pulse which initiates natural convection and makes the independent assessment of the two heat transfer contributions impossible. The different approach of the present study to suppress

the natural convection contribution at low g conditions may be (at least partially) the reason for observing a different behavior than at normal gravity.

The assumption of ignoring the g-jitters on the analysis for the 1st steady state temperature, T_{1ss}, is discussed now. Literature correlations (like Eq. (10) with $m = 0.25$) for an average value of g-jitters of ±0.01 g predict an important contribution of natural convection, i.e., T_{1ss} is not dictated only by conduction. Scaling equation (9) for g-jitters shows that Ra never exceeds 5. This value is in any case much smaller than $Ra_{th} = 40$ found here and this is a confirmation based solely on experimental evidence that during the 1st steady state period only conduction heat transfer is present.

4. Numerical simulations

4.1. Problem set-up

Some theoretical aspects of the problem, based on the results of simulations for conditions similar to the experimental ones, are discussed here. These simulations give the opportunity to assess some scenarios for the discrepancy between the experimental results and the correlations described in the previous section. More specifically, selected experiments covering the whole range of Ra number of the data will be simulated. There are three goals in doing this. (i) To understand better the structure of the temperature and velocity fields in the experimental cell shown in Fig. 1 (information inaccessible experimentally). (ii) To challenge the hypothesis that the appearance of a threshold Ra is due to the finite size of the experimental cell. This might be a possible explanation since the external geometry in the scale of the heater is internal in the scale of the cell. (iii) To assess the dynamics of natural convection onset in order to understand the evolution of the experimental temperature during the transition from microgravity to hypergravity.

The temperature dependence of the liquid's physical properties is not crucial for the purposes of the present study so they can be assumed uniform in the solution domain with their value corresponding to the film temperature, T_f, in each case. The advantage of this assumption is that combined with the conditions $\varepsilon_1 (=\beta\Delta T) \ll 1$, $\varepsilon_2 (=\alpha_h/(L^2 c_p \Delta T)) \ll 1$ (symbols α_h, c_p stand for the thermal diffusivity and specific heat capacity of the liquid, respectively) that are fulfilled in the present experiments, the Boussinesq approximation can be employed [21]. This approximation is employed in the majority of natural convection studies. There are many numerical studies on external geometries in literature (transient or steady state) (e.g. [22]). Many studies refer to thin boundary layers around objects (large Ra number) for which the mathematical problem can be considerably simplified [1]. In the present case such a simplification is not possible because thick boundary layers (small Ra number) are of interest [23,24].

A specific aspect of the present problem is that the geometry is external with respect to the heater but it does not extend to infinity. In fact, it is restricted from the cell walls at a scale much larger than the scale of the heater. It is useful to nondimensionalize the problem before solving it. All variables having units of length are normalized by the characteristic size L, the velocity field is normalized by the natural convection characteristic velocity $U_b = (\gamma L \beta \Delta T)^{0.5}$, pressure is normalized by ρU_b^2, time is normalized by L/U_b and the dimensionless temperature F is given as $F = (T - T_o)/(T_t - T_o)$. Transient simulations for an instantaneous increase of the heater temperature from T_o to T_t are performed here, so T_t is considered to be constant in time. The governing equations have the form [25]:

$$\frac{\partial \vec{u}}{\partial t} + \vec{u}\nabla\vec{u} = \nabla P - F\vec{e}_g + (\mathrm{Pr}/Ra)^{1/2}\nabla^2\vec{u} \tag{12a}$$

$$\frac{\partial F}{\partial t} + \vec{u}\nabla F = (\mathrm{Pr}Ra)^{-1/2}\nabla^2 F \tag{12b}$$

where $\vec{u}$ is the velocity vector and $\vec{e}_g$ is a unity vector in the direction of gravity. The boundary conditions is zero velocity on the heater and on the cell walls, no heat flux on the cell walls and $F = 1$ on the heater walls. The initial condition is $F = 0$ everywhere. A finite element discretization is used with a grid density increasing towards the region of heater. Results from five cases are shown here. Cases 1 and 2 correspond to the conditions of experiments 18 and 12 for FC-72 and cases 3 and 4 correspond to the conditions of experiments 9 and 2 for water. Case 5 is under the same conditions as case 1 but the initial temperature field is not uniform everywhere with $F = 0$. The initial condition for case 5 is a fully developed thermal field around the heater in the presence of conduction alone (i.e., $F = 1$ on heater wall, $Ra = 0$).

4.2. Effect of geometry

The simulations revealed the different way between natural convection and pure conduction, by which the cell temperature increases. In both cases a pseudo steady state temperature profile is established around the heater. Heat is transferred uniformly in the liquid volume in case of conduction. The situation is different in the case of natural convection in which heat is convected by the velocity field and is transferred to the top of the cell so heating of the liquid starts from the top of the cell and moves downward. The simulations performed here reproduce the complicated dynamics described in literature for the case of sphere geometry [22]. In a previous work [4] the finite cell size has been suggested as a possible source of the discrepancy between experiments and correlations based on the results of [23] for the velocity field. In order to check this argument several simulations are performed for decreasing cell diameter until an influence on the Nu number appears. This influence appears for a cell diameter much smaller than the actual one proving that the cell size does not influence the heater dynamics. It is noted that the results presented here are for a cell size 10 times smaller than the actual one (in each direction) having the same temperature field with the actual cell size but a different velocity field. This choice is made for a better description of the velocity profile (recirculation zone).

The steady state isotherms around the heater for case 1 are shown in Fig. 9. The extent of the temperature field in this case is comparable to the heater dimensions. The isotherms are compressed at the one side and expanded at the other side of the heater due to the fluid motion. The steady state temperature profiles at the horizontal plane passing from the centre of the heater are shown in Fig. 10 for cases 1–4 (r is the dimensional radial coordinate). The extent of the temperature field increases as Ra number decreases (as case # increases) but in any case the temperature field does not interfere with the cell walls. The evolution of the temperature profiles in Fig. 10 is rather simple: the profile penetrates into the liquid up to the steady states shown in the figure. A different evolution path is followed in case 5 for which the initial profile corresponds to conduction so the extent of the temperature field is reduced in time toward the steady state which is the same to that of case 1 (Fig. 11). The way of approaching the steady state leaving a tail of slowly reducing temperature, is noteworthy. From Fig. 11 it is apparent that the cell walls do not interfere with the temperature field even in the case of pure conduction (thickest possible temperature boundary layer). The gravity direction velocity component on the equatorial plane of the heater is shown in Fig. 12. The velocity magnitude is of the order of mm/s. The velocity starts from zero at the wall, goes through a maximum value, reduces down to zero and then changes sign due to recirculation, goes through a minimum and finally reaches zero value at the cell

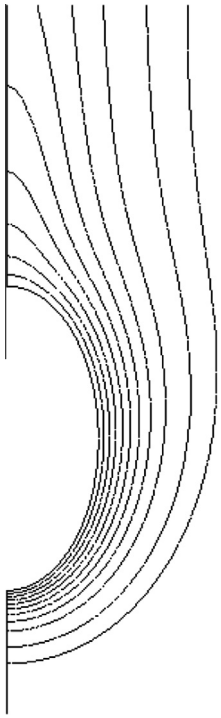

Fig. 9. Steady state isotherms around the heater for case 1 (the isotherms corresponds to the following values of F in increasing distance from the heater: 0.9, 0.8, 0.7, 0.6, 0.5, 0.4, 0.3, 0.2, 0.1, 0.05).

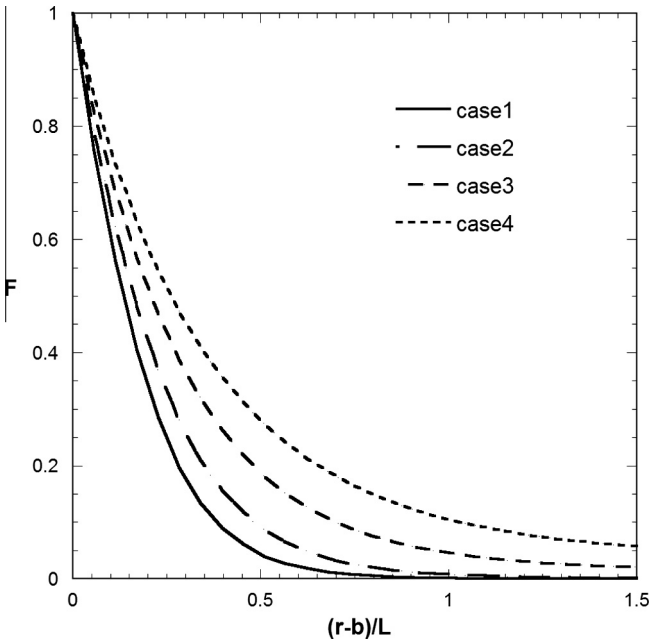

Fig. 10. Pseudo-steady state normalized temperature F profiles on the equatorial plane of the heater vs. normalized distance from the heater wall.

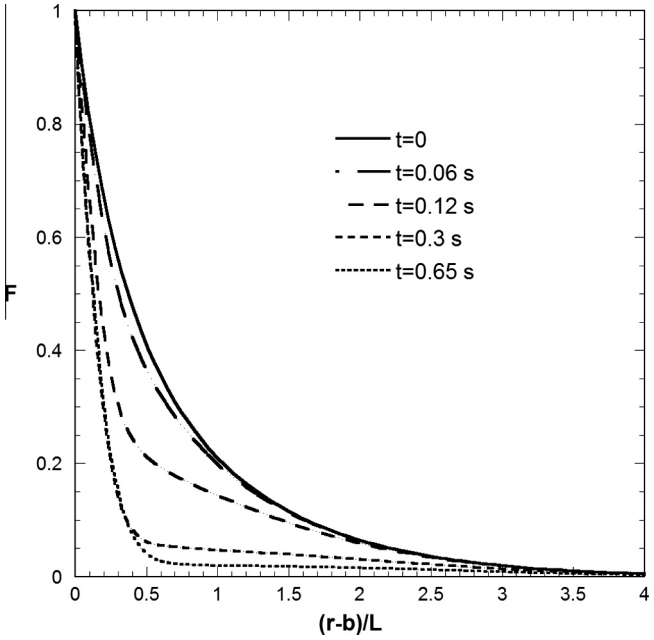

Fig. 11. Evolution of normalized temperature profile on the equatorial plane of the heater for case 5.

wall. Increasing the radius of the cell has negligible influence on the upward velocity profile but a considerable effect on the downward velocity profile which gets broader and with a smaller depth of the minimum. The temperature field is mainly influenced by the velocity field close to the heater and this is the reason that the cell size (for cells larger than this shown here) has no influence on heat transfer characteristics.

The steady state profile of the normal derivative $\frac{\partial F}{\partial \vec{n}}$ (proportional to local heat flux) along the surface of the heater from its lowest to its highest point is shown in Fig. 13. The heat flux increases as *Ra* increases (as case# decreases). The characteristic shape of the curves is due to the combination of natural convection (heat flux rises from the lowest to the highest points of the heater) and conduction (heat flux rises at both tips of the heater due to increased curvature). In case 4 the increase of the conduction contribution leads to loss of the monotonicity of the heat flux curve.

4.3. Natural convection dynamics

The evolution of the instantaneous total Nusselt number for cases 1–5 is presented in Fig. 14. In cases 1–4 the Nusselt number exhibits a singularity at zero time because of the temperature jump of the heater surface. This singularity is due solely to conduction. The natural convection contribution increase in time and the combination of the two mechanisms leads to a minimum in *Nu* evolution curves before the establishment of steady state for cases 1–3 (this behavior is well known in literature e.g. see [13]). The *Nu* number in case 5 starts from its pure conduction value (the value found here is confirmed by comparison with tabulated values from literature), then continues increasing and after a slight overshoot it approaches a steady state which as expected is the same with that of case 1. From the steady state values of the *Nu* number shown in Fig. 14, it can be argued that the finite size of the cell and the heater geometry are not the reasons behind the experimental *H* values of the present work. The computational results confirm qualitatively the existing correlations: there is no threshold Rayleigh number for the water experiments and the *Nu* number (and correspondingly *H*) should increase as *Ra* number increases for FC-72.

The dynamics of natural convection is very fast, actually the time scale to reach what can be practically considered as steady state is about 0.2 s. This fast time scale compared to the several seconds time scale for conduction discussed in [4] is not only due to the larger value of kinematic viscosity than thermal diffusivity but also due to the fact that natural convection is triggered by a

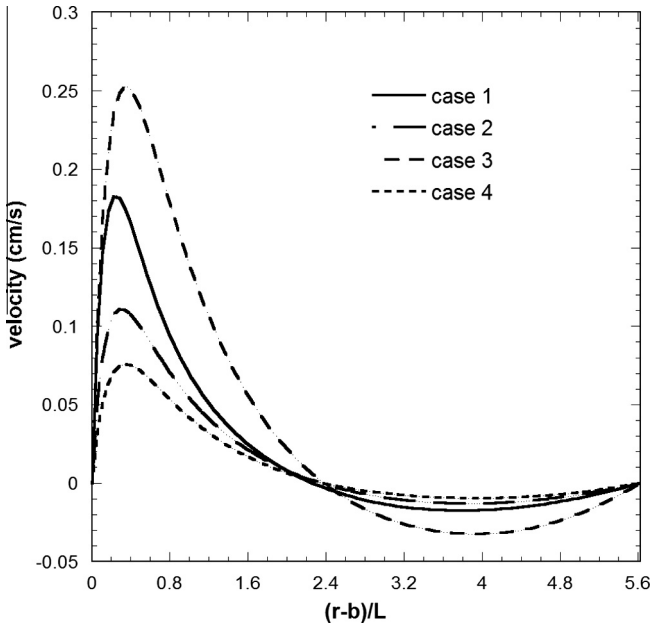

Fig. 12. Velocity component in the direction of gravity on equatorial plane of the heater vs. distance from the heater wall.

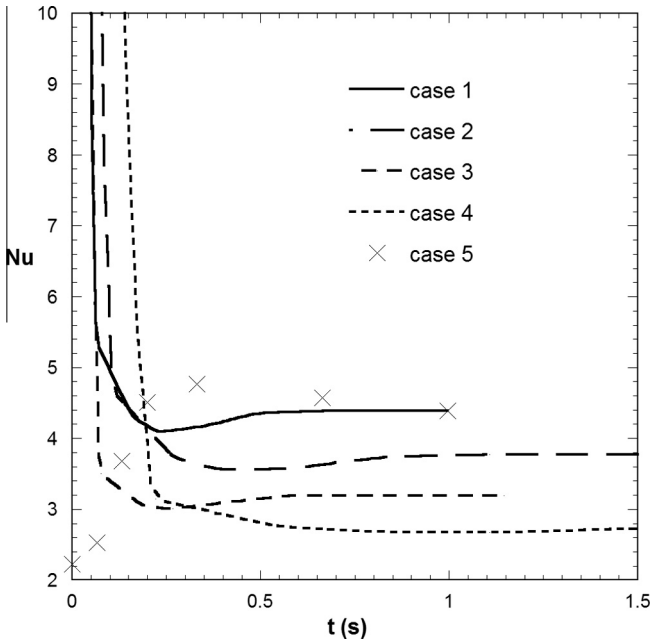

Fig. 14. Evolution of the instantaneous Nusselt number for an instantaneous heat pulse.

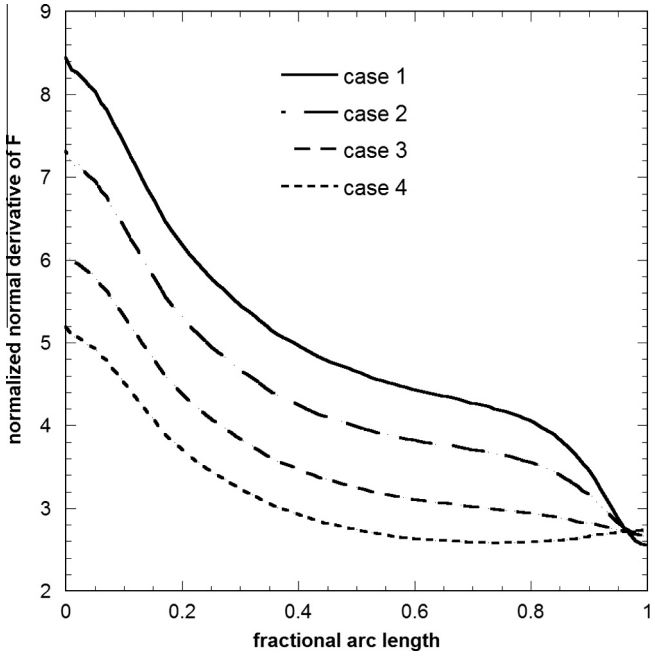

Fig. 13. Profile of normalized normal derivative of F at the surface of heater vs. distance from the lower tip of the heater.

volumetric source (not a surface source as for conduction). This is why the slow convergence to steady state dictated by the $t^{-1/2}$ behavior is avoided. The fast dynamic of the natural convection found here implies that for a variation of γ with characteristic time of 1 s the velocity field and temperature field are adjusted practically instantaneously to this variation acquiring a series of steady states.

Based on the above, the complete evolution of the heater temperature shown in Fig. 3 can be explained as follows: Initially heat is generated in the heater with a temperature dependent rate. Detailed analysis of this period until convergence to steady state can be found in [4]. The slow approach to the steady state is not due to the thermal mass of the heater but to the slow penetration of heat in the liquid, typical for conduction problems. After the approximate establishment of the 1st steady state the gravitational acceleration γ starts to increase from 0 to ~1.6 g and since the thermal capacity of the heater is significant the heater temperature evolution is dictated by the heat source intensity and the steady state Nusselt number that corresponds to the instantaneous γ value. Despite the understanding of the heater temperature dynamics, the strange behavior of the steady state *Nu* found in the previous work [4] is confirmed here by the new experiments. In addition, the present numerical calculations excluded some of the possible reasons suspected previously for this strange behavior. The explanation of the experimental results presented here remains an open subject calling for new ideas.

5. Conclusion

The analysis of the registered steady state temperatures of a miniature heater in a liquid bath of finite size in conditions of zero gravity (~0 g) and hypergravity (~1.6 g) developed during parabolic flights revealed a strange behavior of the Nusselt number (more specifically of the ratio between natural convection and conduction contributions to the Nusselt number). In particular, for water a threshold Rayleigh number is deduced below which no measurable effect of natural convection on heat transfer is observed. On the other hand, for FC-72 the experiments showed a relatively insensitive *Nu* with respect to *Ra* in the range *Ra*: 400–1000. This paradox behavior cannot be explained in terms of existing correlations or numerical computations performed in the present work but it is authentic based on the repeatability and consistency of the present results. A possible source of the discrepancy between the existing knowledge and the present results is that for the first time natural convection is registered independently from conduction by varying the gravitational acceleration. In other words, the role of the gravitational acceleration in existing correlations and theories may need be revised.

References

[1] T. Cebeci, P. Bradshaw, Physical and Computational Aspect of Convective Heat Transfer, Springer-Verlang, New York, 1984.
[2] B. Gebhart, Y. Jaluria, R.L. Mahajan, B. Sammakia, Buoyancy Induced Flow and Transport, Hemisphere Publishing Corporation, New York, 1988.
[3] M. Kaviany, Principles of Heat Transfer in Porous Media, Springer-Verlag, New York, 1991.
[4] M. Kostoglou, S.P. Evgenidis, K.A. Zacharias, T.D. Karapantsios, Heat transfer from small objects in microgravity: experiments and analysis, Int. J. Heat Mass Transfer 54 (2011) 3323–3333.
[5] N. Divinis, T.D. Karapantsios, M. Kostoglou, C.S. Panoutsos, V. Bontozoglou, A.C. Michels, M.C. Sneep, R. de Bruijn, H. Lotz, Bubbles growing in supersaturated solutions at reduced gravity, AIChE J. 50 (2004) 2369–2382.
[6] N. Divinis, T. Karapantsios, R. de Bruijn, M. Kostoglou, V. Bontozoglou, J. Legros, Bubble dynamics during degassing of dissolved gas saturated solutions at microgravity conditions, AIChE J. 52 (2006) 3029–3040.
[7] M. Kostoglou, T.D. Karapantsios, Bubble dynamics during the non-isothermal degassing of liquids. Exploiting microgravity conditions, Adv. Colloid Interface Sci. 134–135 (2007) 125–137.
[8] T.D. Karapantsios, M. Kostoglou, N. Divinis, V. Bontozoglou, Nucleation, growth and detachment of neighboring bubbles over miniature heaters, Chem. Eng. Sci. 63 (2008) 3438–3448.
[9] S. Shafie, N. Amin, G-jitter induced free convection boundary layer on heat transfer from a sphere with constant heat flux, J. Fundam. Sci. 1 (2005) 44–54.
[10] S. Shafie, N. Amin, I. Pop, The effect of g-jitter on double diffusion by natural convection from a sphere, Int. J. Heat Mass Transfer 48 (2005) 4526–4540.
[11] S.P. Evgenidis, K.A. Zacharias, T.D. Karapantsios, M. Kostoglou, Effect of liquid properties on heat transfer from miniature heaters at different gravity conditions, Microgravity Sci. Technol. 23 (2011) 123–128.
[12] P. Moon, D.E. Spencer, Field Theory for Engineers, Van Nostrand Company, New York, 1961.
[13] W.M. Rohsenow, J.M. Hartnett, Y.I. Cho, Heat Transfer Handbook, Mc Graw Hill, New York, 1998.
[14] S.W. Churchill, R. Usagi, A general expression for the correlation of rates of transfer and other phenomena, AIChE J. 18 (1972) 1121–1128.
[15] S.W. Churchill, R. Churchill, A comprehensive correlating equation for heat and component transfer by free convection, AIChE J. 21 (1975) 604–606.
[16] T. Fuji, M. Fujii, T. Honda, A numerical analysis of laminar free convection around an isothermal sphere, Numer. Heat Transfer 4 (1981) 68–84.
[17] G.D. Raithby, K.G.T. Hollands, A general method of obtaining approximate solutions to laminar and turbulent free convection problems, Adv. Heat Transfer 11 (1975) 265–315.
[18] T. Yuge, Experiments on heat transfer from spheres including combined natural and forced convection, J. Heat Transfer 82C (1960) 214–220.
[19] J.E. Boberg, P.S. Starret, Determination of free convection heat transfer properties of fluids, Ind. Eng. Chem. 50 (1958) 807–810.
[20] W.S. Amato, C. Tien, Free convection heat transfer from isothermal spheres in water, Int. J. Heat Mass Transfer 15 (1972) 327–339.
[21] J.M. Mihaljan, A rigorous exposition of the Boussinesq approximation applicable to a thin layer of fluid, Astrophys. J. 136 (1962) 1126–1133.
[22] H. Jia, G. Gogos, Transient laminar natural convection heat transfer from isothermal spheres, Numer. Heat Transfer Part A: Appl. 29 (1996) 83–101.
[23] H. Jia, G. Gogos, Laminar natural convection heat transfer from isothermal spheres, Int. J. Heat Mass Transfer 39 (1996) 1603–1615.
[24] V.N. Kurdyumov, A. Linan, Free convection from a point source of heat and heat transfer from spheres at small Grashof number, Int. J. Heat Mass Transfer 42 (1999) 3849–3860.
[25] W.M. Deen, Analysis of Transport Phenomena, Oxford University Press, London, 1998.